Weierstraß-Institut
für Angewandte Analysis und Stochastik

im Forschungsverbund Berlin e.V.

Preprint ISSN 0946 – 8633

Asymptotic pulse shapes in filamentary propagation of intense femtosecond pulses

Carsten Krüger [1], Ayhan Demircan[1], and Günter Steinmeyer [2]

submitted: 15. Sept. 2008

[1] Weierstrass Institute
for Applied Analysis
and Stochastics
Mohrenstraße 39
10117 Berlin, Germany

[2] Max Born Institute
for Nonlinear Optics
and Short Pulse Spectroscopy
Max-Born-Straße 2A
12489 Berlin, Germany

No. 1359
Berlin 2008

2000 *Mathematics Subject Classification.* Primary 78A60, 81V80, 35Q55, 37K40 .

Key words and phrases. Nonlinear Schrödinger equations; Optical self-focusing; Ultrashort pulse propagation.

.

Edited by
Weierstraß-Institut für Angewandte Analysis und Stochastik (WIAS)
Mohrenstraße 39
10117 Berlin
Germany

Fax: + 49 30 2044975
E-Mail: preprint@wias-berlin.de
World Wide Web: http://www.wias-berlin.de/

Abstract

Self-compression of intense ultrashort laser pulses inside a self-guided filament is discussed. The filament self-guiding mechanism requires a balance between diffraction, plasma self-defocusing and Kerr-type self-focusing, which gives rise to asymptotic intensity profiles on axis of the filament. The asymptotic solutions appear as the dominant pulse shaping mechanism in the leading part of the pulse, causing a pinch of the photon density close to zero delay, which substantiates as pulse compression. The simple analytical model is backed up by numerical simulations, confirming the prevalence of spatial coupling mechanisms and explaining the emerging inhomogeneous spatial structure. Numerical simulations confirm that only spatial effects alone may already give rise to filament formation. Consequently, self-compression is explained by a dynamic balance between two optical nonlinearities, giving rise to soliton-like pulse formation inside the filament.

1 Introduction

Opening a new avenue towards compression of multi-mJ few cycle pulses, nonlinear optical processes in self-guided filamentary geometries have recently seen a strongly revived interest. Hauri et al. pioneered this application, loosely focusing 840 μJ pulses from a Ti:sapphire system into argon gas, which resulted in compression of 43 fs pulses down to about 6 fs [1]. Compared to hollow fiber compressors [2], self-guiding filament compression does neither exhibit coupling losses nor is it limited by potential damage to the guiding structure. Filament self-guiding arises from a balance of the self-focusing Kerr effect and a complementary defocusing effect from plasma generation via multiphoton ionization, locking the beam profile at a few hundred micron diameter for propagation lengths exceeding the Rayleigh range of a Gaussian beam with equal diameter [3, 4]. While the early work of Hauri still required chirped mirrors for dispersion compensation, pure self-compression of multi-mJ pulses to below 10 fs pulse duration has been subsequently experimentally demonstrated, obliterating the requirement for any external dispersion compensation scheme [5]. Under other experimental conditions, self-compression has also been found in strongly ionized gases [6] or at much longer pulse durations [7]. The potential of filaments to compress pulses directly into the few-cycle range had been predicted in numerical simulations [8, 9, 10] and more specifically analyzed in Ref. [11]. These numerical simulations clearly identify self-steepening and plasma defocusing as primary effects shaping the trailing part of the pulse in the filamentary channel. However, no effect has yet been isolated to explain shaping in the leading part of

the pulse. This part often exhibits a pedestal structure and typically rises much slower than the falling edge drops. These characteristic asymmetric pulse shapes have clearly been observed both, in experiment and numerical simulations. Their exact origin, however, is still unclear.

To clear up the origins of filamentary self-compression, in Sec. 1 we present a simple analytical model leading to predictions on the temporal shape of the self-stabilizing intensity profiles. In Sec. 2, we present numerical evidence that filamentation can already be reached in a simplified model, including only Kerr and plasma nonlinearities, identifying spatial effects as key players for the formation of stable filaments. Finally, in Sec. 3 we compare these results to numerical simulations of the full model equations.

2 Analytical predictions for asymptotic pulse shapes

In the following, we identify the pedestal-like asymmetric self-compressed pulses as arising from an asymptotic solution for the pulse shape, stemming from a dynamic balance between plasma-induced defocusing and Kerr-type self-focusing. This balance is typically considered the prevalent mechanism for the appearance of spatially stable beam profiles [3, 4], and it has to be met in every temporal point of a short pulse to ensure self-confined propagation of the pulse beyond the Rayleigh range. On the central axis of the filament, a dynamic balance between Kerr-induced refractive index changes and those arising from multiphoton ionization leads to self-guiding when the following condition [3, 12] between intensity profile $I(t)$ and beam radius $w_0(t)$ is met

$$n_2 I(t) = \frac{\rho_0}{2\rho_c} \int_{-\infty}^{t} W[I(t')]\mathrm{d}t' + \frac{n_2 P_{\mathrm{cr}}}{\pi w_0(t)^2}. \tag{1}$$

Here

$$\rho_c := 4\pi^2 c^2 \frac{m_e \epsilon_0}{\lambda_0^2 q_e^2} \tag{2}$$

is the critical plasma density calculated from Drude theory, ρ_0 the number density of atoms in the nonlinear medium. The factor $\rho_0/2\rho_c$ converts from ionization probability of an individual atom to the resulting change in refractive index, where ρ_0 is the number density of atoms in the nonlinear medium. n_2 is the nonlinear index of refraction, q_e and m_e are electron charge and mass, respectively, ϵ_0 is the dielectric constant, c the speed of light, λ_0 the wavelength. Finally, we define the critical power for self-focusing as $P_{\mathrm{cr}} = 0.146\lambda_0^2/n_2$ [13]. Despite its simplicity, the self-guiding model Eq. (1) has been confirmed to describe intensities and electron densities inside the filament channel remarkably well, even when setting $w_0 = \text{const.}$, thereby neglecting filament radius variations [12]. In this case, using a simple multiphoton expression for the ionization rate

$$W_{\mathrm{MPI}} = \sigma_{N^*} I^{N^*} \tag{3}$$

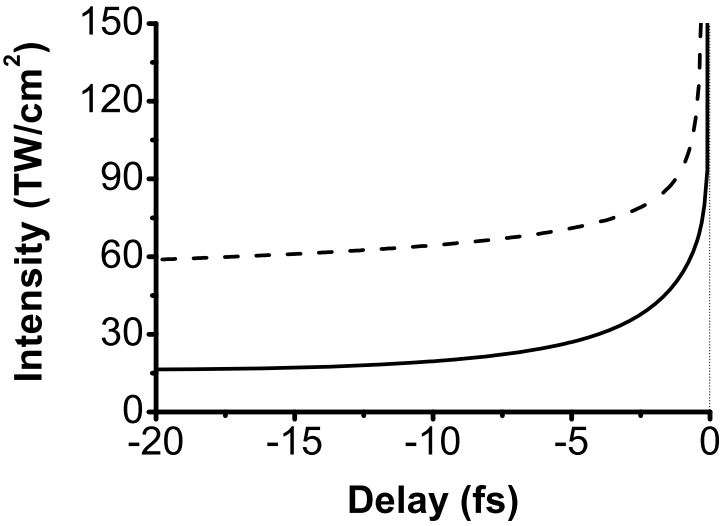

Figure 1: Asymptotic pulse shapes in the filament: Solution of Eq. (1) with (solid line) and without (dashed line) diffraction term for argon.

gives rise to root-like solutions of Eq. (1),

$$I(t) \propto (-t)^{1/(1-N^*)}, \tag{4}$$

as indicated by the dashed line in Fig. 1. For computation of the data we used $N^* = 8.51$, $\sigma_{N^*} = 3.6 \times 10^{-108}\,\mathrm{cm}^{2N^*}\mathrm{W}^{-N^*}\mathrm{s}^{-1}$ as a local fit to ADK theory [14, 15]. These solutions already exhibit the characteristic asymmetry of the pulses observed in the experiments [5, 11] with a slowly rising pedestal-like leading edge and a sharp falling edge that may additionally be shaped by self-steepening effects. As Eq. (1) imposes a balance between an instantaneous and a cumulative effect on the phase, the solution must be monotonously growing with respect to t. Other than solitonic solutions of the nonlinear Schrödinger equation, the solutions of Eq. (1) are not localized and exhibit a pole at $t = 0$. Removing the simplifying assumption of a constant beam diameter, one can solve Eq. (1) for any given input power profile $P(t)$, utilizing $w_0(t) = [P(t)/\pi I(t)]^{1/2}$. Using ADK theory for computation of $W[I]$ and a Gaussian pulse shape with $t_0 = 45\,\mathrm{fs}$ pulse duration (FWHM) and 3 P_{cr} peak power, we calculate the solution depicted as a solid line in Fig. 1. This solution shows the same symmetry and the same root-like functional dependence as under the constant diameter assumption, however, at a strongly reduced apparent $N^* \approx 2-4$ in Eq. (4) compared to MPI theory. This reduction of the root index shapes out as a strongly reduced pedestal, which brings these solutions closer to the shapes experimentally observed and seen in full numerical simulations [11].

The solutions depicted in Fig. 1 do not only constitute solutions to Eq. (1), yet more importantly, small deviations from the ideal solution will induce negative feedback, i.e., the nonlinear mechanisms will automatically correct perturbations from the

ideal pulse shape. If, for example, the intensity exceeds the solution $I(t)$ of Eq. (1) by $+\Delta I$ for a duration τ, this deviation creates excess electrons. As plasma generation grows much faster with intensity than the Kerr effect, defocusing forces prevail over a slightly enhanced self-focusing effect. Consequently, the intensity reduces owing to an increasing w_0, reestablishing the balance of focusing and defocusing effects. Similarly, plasma generation will quickly stall for a negative deviation $-\Delta I$, again reestablishing the balance and increasing the intensity via shrinking w_0. Perturbing Eq. (1), the restoration of the balancing solution demands that plasma effects overrule Kerr contributions, i.e., that

$$n_2 \Delta I < \frac{\rho_0}{2\rho_c} \frac{\partial W}{\partial I} \Delta I \tau \approx \frac{\rho_0 N^*}{2\rho_c} \sigma_{N^*} I^{N^*-1} \Delta I \tau \tag{5}$$

be fulfilled for a given duration τ of the perturbation. As a criterion for the strength of the self-compression effects, we determine the smallest possible τ for the above inequality to hold and find remarkably little variation with wavelength and gas [16], which clearly underlines the universality of the observed self-compression phenomenon [17, 18]. However, the stability analysis also clearly points out that filament self-compression only becomes active when initial power levels are sufficiently high, which may explain why a more traditional pulse compression route was pursued in early experiments. Stability of Eq. (1) against perturbations makes its solutions asymptotic ones. Upon extended propagation, the on-axis intensity profile therefore converges against this asymptotic solution, similar to the formation of fiber solitons if only the energy of the fundamental temporal soliton is exceeded. In contrast to the latter, however, the shaping mechanism inside the filament is of spatial nature, with excess energy being stripped off into the reservoir surrounding the core of the filament whereas fiber solitons transfer their excess energy into a temporal continuum.

Despite the proven stability of the soliton-like solutions of Eq. (1), it is yet unclear whether typical propagation lengths in the filament suffice for substantial reshaping of the intensity profile towards its asymptotic solution.

3 Numerical simulations of a reduced model leading to filamentary propagation

In order to substantiate our analytical results with numerical data, we use a radially symmetric evolution model for envelope of the light electric field $\mathcal{E}(r, z, t)$ [11]. For an isolation of spatial shaping mechanisms, we suspended temporal dispersion, few-cycle corrections and dissipative effects in the model and only included Kerr nonlinearity, plasma nonlinearity and linear diffraction. This effectively eliminates all coupling mechanisms leading to exchange of energy between adjacent temporal sections of the pulse. The field envelope $\mathcal{E}$ and the density of plasma ρ generated

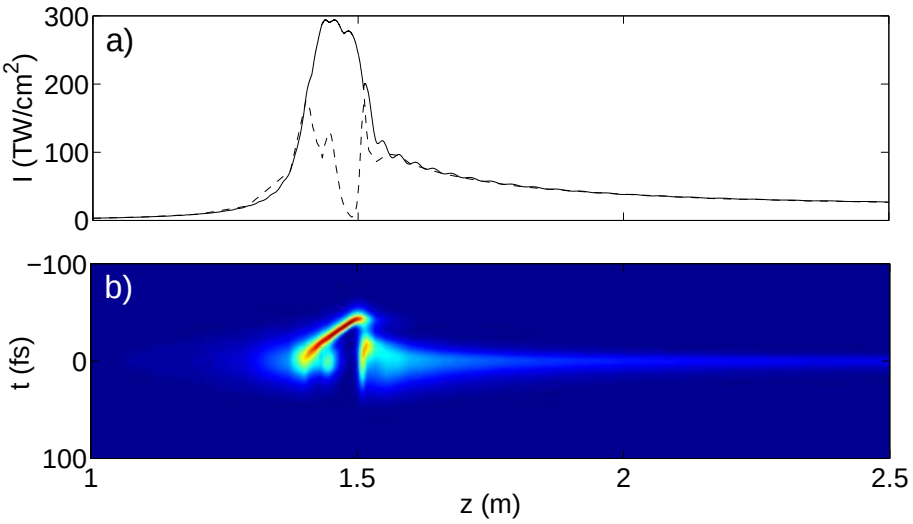

Figure 2: a) Evolution of the peak intensity along the propagation direction z (solid line). The dashed line corresponds to the evolution of $I(t=0, r=0)$ b) Evolution of the on-axis temporal intensity profile. A soliton-like structure emerges at about $z = 1.6$ m.

by multiphoton or tunneling ionization evolve as

$$\partial_z \mathcal{E} = \frac{i}{2k_0}\Delta_\perp \mathcal{E} + i\frac{\omega_0}{c} n_2 |\mathcal{E}|^2 \mathcal{E} - i\frac{k_0}{2\rho_c}\rho(\mathcal{E})\mathcal{E}, \tag{6}$$

$$\rho(\mathcal{E}) = \rho_{nt}\left(1 - \exp\left(-\int_{-\infty}^{t} dt' W[I]\right)\right) \tag{7}$$

where $I = \mathcal{E}^*\mathcal{E}$ is the intensity of the laser beam. To reestablish experimental conditions in [5], we choose $n_2 = p \times 10^{-19}\mathrm{cm}^2/\mathrm{W}$ for modeling argon, a density $\rho_0 = p \times 2.7 \times 10^{19}\,\mathrm{cm}^{-3}$, and a pressure $p = 30\,\mathrm{kPa}$. The ionization rate $W[\mathcal{E}]$ in argon for the relevant intensity range is calculated according to ADK theory for tunneling ionization [14]. The incident field is modeled as a Gaussian in space and time ($w_0 = 5.5\,\mathrm{mm}$, $t_0 = 45\,\mathrm{fs}$), being subsequently focused into the medium an $f = 1.5\,\mathrm{m}$ lens. The peak input power was set to $P = 5P_{\mathrm{cr}}$.

The result of these simulations clearly illustrates that spatial effects alone already suffice for the formation of a filament, as the evolution of the maximum intensity along z depicted in Fig. 2a) shows. Passing through the focus, the time slice with maximum intensity is shifted back and forth in time, as is illustrated by the dashed line in Fig. 2a) and even more clearly by the evolution of the on-axis temporal intensity profile shown in Fig. 2b). This process continues until at $z = 1.6\,\mathrm{m}$ a soliton-like structure emerges. A more detailed illustration of the pulse-shaping processes in the vicinity of the focus is given by the sequence of pulses in the (t, r)-plane depicted in Fig. 3(a-d). Approaching the nonlinear focus, the pulse strips off energy into a spatial reservoir and a system of spatial rings develops at about $z = 1.45\,\mathrm{m}$. At $z = 1.5\,\mathrm{m}$, the trailing part of the pulse refocuses, while the leading

part defocuses. The stable filamentary pulse thus formed during passage through the focus exhibits a small leading sub-pulse at negative delays, while the main portion of the pulse is shifted towards positive delays, with a very steep leading edge. Closer inspection of this data also shows pulse self-compression during the stage of filamentary propagation. The evolution of on-axis temporal pulse profiles

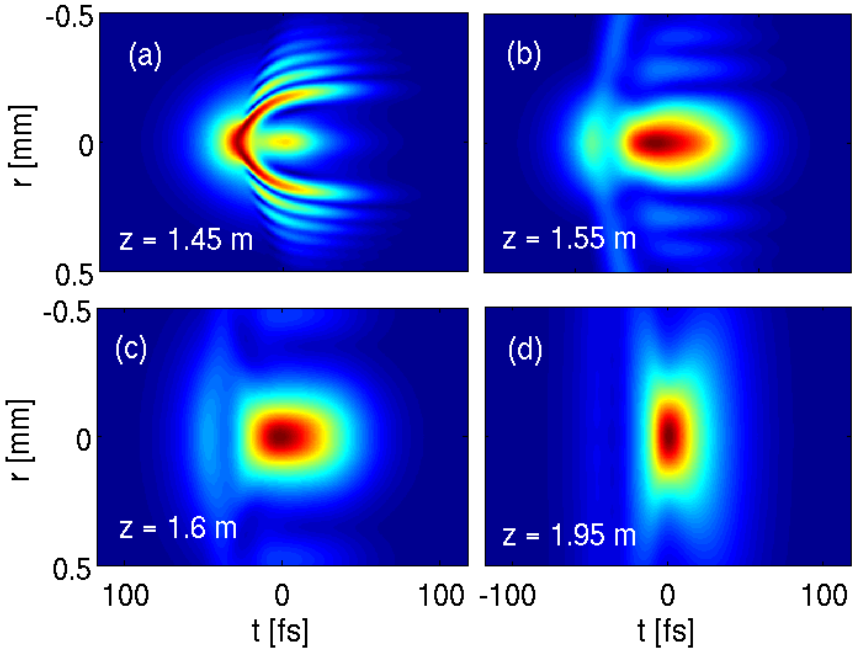

Figure 3: Sequence of pulses in the (t, r) representation. A strip-off of energy into a system of spatial rings can be observed as the pulses passes the focus. A stable soliton-like structure with characteristic temporal asymmetry emerges at about $z = 1.6\,\mathrm{m}$.

is shown in Fig. 4(a), clearly revealing compression of the initial pulse shape (solid line, $z = 1.7$ m) toward gradually shorter duration (dashed line, $z = 1.8$ m and dash-dotted line, $z = 1.9$ m). The intensity distribution of the soliton-like pulses in the (t, r) plane in Fig. 4b) and Fig. 3d) furthermore reveals a pinched structure in the region of maximum intensity and a characteristic temporal asymmetry. Interestingly, this characteristic structure can be observed in the numerics for a wide range of initial conditions, provided only that a stable filament is formed. We conclude that spatial deformation of the beam profile is, in fact, capable of driving the on-axis intensity profile toward the asymptotic solution within a few centimeters of propagation through the filament channel.

4 Comparison with the full numerical model

To this point, our analysis has concentrated on spatial effects and completely neglected effects like dispersion and self-steepening that may cause an energy flow

between adjacent temporal slices of the pulse. This reduction appears reasonable in the slowly rising, leading part of the pulse, the shaping of which is our strongest concern. To convince ourselves that spatial effects dominate in this part of the pulse and that soliton-like structures also appear in complete simulations of the scenario, we pursued full simulations of the filament propagation, including few-cycle corrections, space-time focusing, and dissipative effects, cf. Ref. [11]. In the full model, the envelope $\mathcal{E}$ and the plasma density ρ evolve according to

$$\partial_z \mathcal{E} = \frac{i}{2k_0} T^{-1} \Delta_\perp \mathcal{E} + i\mathcal{D}\mathcal{E} + i\frac{\omega_0}{c} n_2 T |\mathcal{E}|^2 \mathcal{E}$$
$$-i\frac{k_0}{2\rho_c} T^{-1} \rho(\mathcal{E})\mathcal{E} - \frac{\sigma}{2}\rho\mathcal{E} - \frac{U_i W(I)(\rho_{nt} - \rho)}{2I}\mathcal{E}, \tag{8}$$

$$\partial_t \rho = W(I)(\rho_{nt} - \rho) + \frac{\sigma}{U_i}\rho I \tag{9}$$

Here, the operator $\mathcal{D}$ models nonlinear dispersion in argon, and $T = 1 + \frac{i}{\omega_0}\partial_t$ introduces few-cycle corrections. Further on, $\sigma = p \times 10^{-19}\mathrm{cm}^2$ is the inverse Bremsstrahlung cross section and $U_i = 16\,\mathrm{eV}$ the ionization potential of argon. As shown with the pulse sequence in Fig. 4c) and the evolution of the maximum

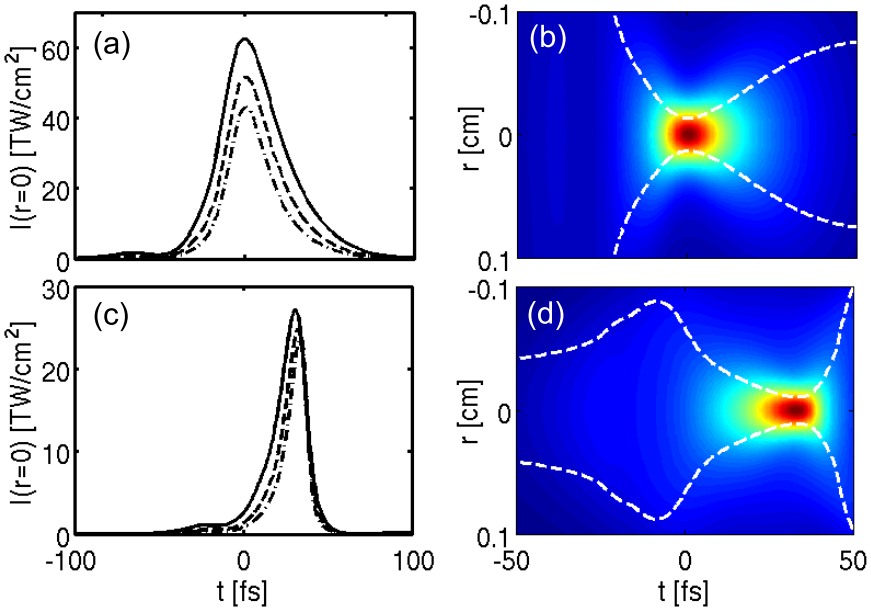

Figure 4: (a) Sequence of on-axis temporal intensity profiles in the filamentary channel, reduced model (b) (t, r) representation of a pulse in the filamentary channel, reduced model (c) Sequence of pulses in the full numerical model governed by Eq. (8). (d) Soliton-like structure in the full numerical model.

intensity and the on-axis temporal profile in Fig. 5a), minor adjustment of parameters suffices to see pulse self-compression within the full model equations. Here self-steepening provides a much more effective compression mechanism in the trailing part, however, with nearly unchanged behavior in the leading part of the pulse.

Otherwise, these pulses exhibit the same characteristic asymmetry and similar intensity levels as in the analytic solutions. Quite clearly, energy exchange between neighboring temporal sections of the pulse is not negligible, in particular in the steep trailing edge where it clearly dominates. Otherwise, however, temporal effects have only a modifying effect. Despite the extreme complexity of the filament scenario, our

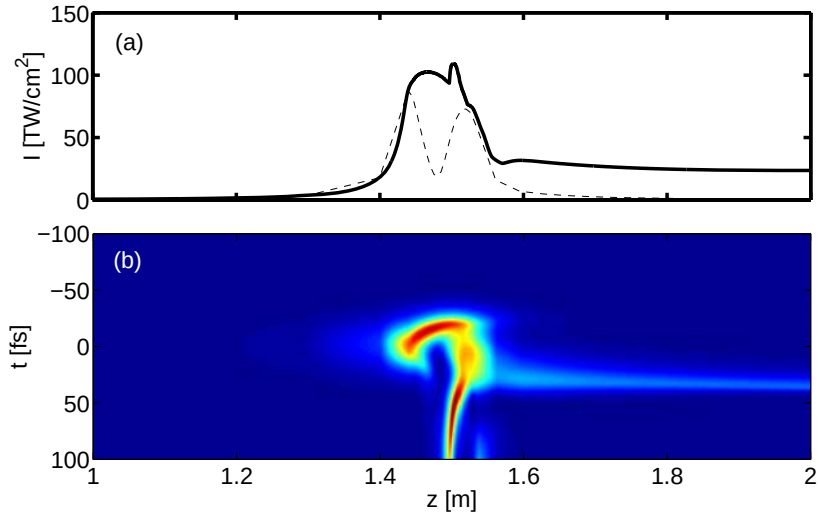

Figure 5: (a) Evolution of the maximum on-axis intensity along z for the full numerical model Eq. (8) (solid-line) and evolution of $I(t = 0, r)$ along z (dashed line).

analytical model isolates a rather intuitive picture for the major mechanisms leading to the recently observed self-compression of few-cycle pulses. While the trailing part of the pulse is dominantly shaped by self-steepening, the other half evolves in a soliton-like fashion towards an asymptotic pulse shape. In this process radial energy flow leads to a concentration or deconcentration of energy on the axis of propagation and gives rise to a characteristic spatio-temporal shapes of the pulse. As can clearly be seen in Fig. 4d), the pinching of the pulses inside the filament therefore causes the strongest intensity increase close to the discontinuity-like trailing edge, being shaped by self-steepening effects. Apart from being coupled by the integral in Eq. (1), there is only negligible energy exchange between adjacent temporal slices in the leading edge of the pulse, which sets filament compression apart from traditional laser pulse compression [19]. In fact, we find that the self-compression scenario is related more closely to soliton compression [20], yet with the compression mechanism arising from the dynamic balance of two nonlinear effects rather than that of dispersion and self-phase modulation. This dynamic balance gives rise to the discussed new class of soliton-like pulse shaping effects, even if the awkward mathematical structure of the root-like solution [Eq. (4)] cannot formally be considered a localized wave.

From the viewpoint of applications, however, the pinch-like structure of Fig. 4d) restricts self-compression to the spatial center of the filament [11]. For certain applications, it therefore appears advisable not to use self-compression but to stick to the traditional spectral-broadening dispersion-compensation scheme [1], as a barely

measurable radial dependence of pulse duration will result [21]. Given the universal nature of the self-compression phenomenon, however, a spatial structure appears tolerable in the ultraviolet range, as dispersion compensation becomes a challenging task at in the uv. Additionally, soliton-like compression effects may well explain some of the already demonstrated remarkably simple generation of sub-10 fs pulses at 300 nm inside a filament [17], the potential for even shorter pulses [22], and substantial self-compression observed in the infrared [18].

5 Conclusion

In conclusion, we explained pulse self-compression as a novel soliton-like pulse shaping effect in plasmas, with the noted difference of stemming from the balance of two competing nonlinear optical effects. While traditional pulse compression mechanisms utilize longitudinal energy concentration, the effects underlying filament self-compression act radially and cause self-pinching of the pulse's beam profile. Nevertheless, pulse self-compression enables the most efficient energy concentration of femtosecond laser pulses at kHz repetition demonstrated to date. Ultimately, we believe that revealing the structures behind this remarkably powerful mechanism opens up an avenue to novel applications of nonlinear plasma optics for few-cycle pulse generation in otherwise inaccessible wavelength regions.

Acknowledgements

Financial support by the Deutsche Forschungsgemeinschaft, grants DE 1209/1-1 and STE 762/7-1, is gratefully acknowledged

References

[1] C. P. Hauri, W. Kornelis, F. W. Helbing, A. Heinrich, A. Couairon, A. Mysyrowicz, J. Biegert, and U. Keller, Appl. Phys. B **79**, 673 (2004).

[2] M. Nisoli, S. De Silvestri, O. Svelto, R. Szipőcs, K. Ferencz, C. Spielmann, S. Sartania, and F. Krausz, Opt. Lett. **22**, 522 (1997).

[3] A. Braun, G. Korn, X. Liu, D. Du, J. Squier, and G. Mourou, Opt. Lett. **20**, 73 (1995).

[4] A. Brodeur and S. L. Chin, J. Opt. Soc. Am. B **16**, 637 (1999).

[5] G. Stibenz, N. Zhavoronkov, and G. Steinmeyer, Opt. Lett. **31**, 274 (2006).

[6] N. L. Wagner, E. A. Gibson, T. Popmintchev, I. P. Christov, M. M. Murnane, and H. C. Kapteyn, Phys. Rev. Lett. **93**, 173902 (2004).

[7] I. G. Koprinkov, A. Suda, P. Wang, and K. Midorikawa, Phys. Rev. Lett. **84**, 3847 (2000).

[8] A. L. Gaeta, Phys. Rev. Lett. **84**, 3582 (2000).

[9] L. Bergé and A. Couairon, Phys. Rev. Lett. **86**, 1003 (2001).

[10] S. Champeaux and L. Bergé, Phys. Rev. E **68**, 066603 (2003).

[11] S. Skupin, G. Stibenz, L. Bergé, F. Lederer, T. Sokollik, M. Schnürer, N. Zhavoronkov, and G. Steinmeyer, Phys. Rev. E **74**, 056604 (2006).

[12] A. Couairon and A. Mysyrowicz, Phys. Rep. **441**, 47 (2005).

[13] R. W. Boyd, *Nonlinear Optics*, (2nd ed., Academic Press, San Diego, CA, 2003).

[14] M. V. Ammosov, N. B. Delone and V. P. Krainov, Sov. Phys. JETP **64**, 1191 (1986).

[15] T. Brabec and F. Krausz, Rev. Mod. Phys. **72**, 545 (2000).

[16] H. J. Lehmeier, W. Leupacher and A. Penzkofer, Opt. Commun. **56**, 67 (1985).

[17] S. A. Trushin, K. Kosma, W. Fuß, and W. E. Schmid, Opt. Lett. **32**, 2432 (2007).

[18] C. P. Hauri *et al.*, Opt. Lett. **32**, 868 (2007).

[19] E. B. Treacy, IEEE J. Quantum Electron. **5**, 454 (1969).

[20] K. Smith and L. F. Mollenauer, Opt. Lett. **14**, 751 (1989).

[21] A. Zaïr *et al.*, Opt. Express **15**, 5394 (2007).

[22] L. Bergé and S. Skupin, Opt. Lett. **33**, 750 (2008).